factors were refined for the hydrogen atoms: one for the three *n*-propyl groups and one for the three cyclopentadienyl ligands for each of the two independent molecules in the asymmetric unit. The refinement converged with $R = 0.0304$ and $R_w = 0.0268$. A total of 545 parameters were refined, giving an observation to parameter ratio of 17.0; the largest shift/error in the final cycles was 0.068. A final difference electron density map showed no significant residual features: $\partial\rho_{max}$, 0.80 e Å^{-3}; $\partial\rho_{min}$, −0.69 eÅ^{-3}.

Acknowledgment. We thank the Natural Sciences and Engineering Research Council of Canada and the Quebec Department of Education for financial support and for scholarships to P.-Y.P. Stephen van Loggerenberg, of PGM Chemicals Ltd. is thanked for a generous gift of $RuCl_3 \cdot H_2O$. Helpful discussions with Dr. Jim Britten, formerly of the Department of Chemistry, McGill University, concerning the X-ray structural analysis are gratefully acknowledged.

Registry No. **1a**, 139041-61-5; **1b**, 139041-62-6; **4**, 139041-63-7; $CpRu(PPh_3)_2S\text{-}1\text{-}C_3H_7$, 126899-34-1; $CpRu(PPh_3)_2SCHMe_2$, 126899-35-2.

Supplementary Material Available: An ORTEP drawing of $[CpRuS\text{-}1\text{-}C_3H_7]_3$ showing the numbering scheme for molecule B (Figure 4), a full-length table of crystallographic data (Table IV), a table of anisotropic temperature factors (Table V), a table of calculated atomic coordinates and common isotropic temperature factors of the hydrogen atoms of $[CpRuS\text{-}1\text{-}C_3H_7]_3$ (Table VI), and a table of bond lengths and angles (Table VII) (13 pages); a table of observed and calculated structure factors (Table VIII) (55 pages). Ordering information is given on any current masthead page.

Contribution from the Department of Chemistry, University of California, Davis, California 95616

Neutral Catecholate Derivatives of Manganese and Iron: Synthesis and Characterization of the Metal–Oxygen Cubane-like Species $M_4(DBCat)_4(py)_6$ (M = Mn, Fe), the Trinuclear Complex $Mn_3(DBCat)_4(py)_4$, and the Dimers $M_2(DBCat)_2(py)_n$ (M = Mn, *n* = 6; M = Fe, *n* = 4, 6)

Steven C. Shoner and Philip P. Power*

Received May 22, 1991

The synthesis and characterization of several new catecholate derivatives of manganese and iron are described. The reaction of 3,5-di-*tert*-butylcatechol ($DBCatH_2$) with the amides $M[N(SiMe_3)_2]_2$ (M = Mn, Fe) in the presence of pyridine (py) affords the title compounds in high yield. The dimers $Mn_2(DBCat)_2(py)_6$ (**1**) and $Fe_2(DBCat)_2(py)_n$ (*n* = 4 (**4a**), 6 (**4b**)) are obtained by treatment of catechol with the appropriate amide in pyridine. In hexane or toluene, this reaction gives the tetrametallic species $M_4(DBCat)_4(py)_6$ (M = Mn (**2**), Fe (**5**)) upon the addition of 2 equiv of pyridine or, in the case of **2**, by recrystallization of the dimer from toluene. $Mn_3(DBCat)_4(py)_4$ (**3**) is obtained by slow air oxidation of **2** or by addition of $^1/_3$ equiv of 3,5-di-*tert*-butyl-*o*-benzoquinone to the reaction of $Mn[N(SiMe_3)_2]_2$ with $DBCatH_2$ in hexane with subsequent addition of pyridine. Compounds **1–5** were characterized by infrared, UV–visible, ^{1}H NMR, and EPR spectroscopy and X-ray crystallography. The crystal structures of **1**, **4a**, and **4b** (which cocrystallize as **4**) consist of centrosymmetric dimeric units in which both catecholate ligands bridge the two metal centers by one doubly bridging and one terminal oxygen. Three pyridine ligands per metal complete the distorted octahedral geometry in **1** and **4a**. In **4b** two pyridines are bound to each iron which have distorted trigonal bipyramidal geometry at the metal. The structure of **2** possesses a Mn_4O_6 core composed of four doubly bridging oxygens, two triply briding oxygens, and four manganese atoms. Further coordination by pyridine ligands gives rise to two manganese centers with trigonal bipyramidal geometry and two with distorted octahedral geometry. The overall geometry of the complex gives **2** a basket-like appearance. Compound **5** has an Fe_4O_4 distorted cubane core, with each iron bound to three triply bridging oxygens and one terminal oxygen. As in **2**, the six pyridine ligands are arranged to give two octahedral and two trigonal bipyramidal metal centers. The structure of **3** consists of two five-coordinate Mn(III) centers (one square pyramidal and one trigonal bipyramidal), each bound by two doubly bridging catecholate oxygens to a central pseudooctahedral Mn(II) ion. The cis arrangement of the bridging units imposes a bent geometry on the compound. Spectroscopic studies suggest that complex **3** undergoes intramolecular electron transfer on dissolution in toluene to give the all-Mn(II) semiquinone form $Mn_3(DBSQ)_2(DBCat)_2(py)_4$.

Interest in the chemistry of manganese and iron catecholate and semiquinonate complexes has greatly increased in recent years.[1-5] One reason for this has been the recognition of the important role of quinone- and catechol-containing groups in biology. For instance, the use of catecholate-containing sequestering agents[2] by various organisms to concentrate V^{4+} and Fe^{3+} ions has been established[3-5] and successfully modeled in recent years.[6-8] Manganese and iron plastoquinone complexes have been implicated as the electron-accepting center in photosystem II[9-11] in plants and some photosynthetic bacteria, as well as many other biological electron-transport chains.[13,14] Catechol dioxygenase enzymes containing iron or copper are known to oxidize catechol

(1) Thompson, R. H. *Naturally Occurring Quinones*; Academic Press: New York, 1971.
(2) Raymond, K. N. *Coord. Chem. Rev.* **1990**, *105*, 135.
(3) Lee, S.; Kustin, K.; Robinson, W. E.; Frankel, R. B.; Spartalian, K. *J. Inorg. Biochem.* **1988**, *33*, 183.
(4) Matzanke, B. F.; Müller-Matzanke, G.; Raymond, K. N. *Iron Carriers and Iron Proteins*; Loehr, T. M., Ed.; Physical Bioinorganic Chemistry Series; VCH Publishers: New York, 1989; p 1.
(5) Smith, M. J.; Kim, D.; Horenstein, B.; Nakanishi, K.; Kustin, K. *Acc. Chem. Res.* **1991**, *24*, 117.
(6) Bulls, A. R.; Pippin, C. G.; Hahn, F. E.; Raymond, K. N. *J. Am. Chem. Soc.* **1990**, *112*, 2627.
(7) Garrett, T. M.; McMurry, T. J.; Hosseini, M. W.; Reyes, Z. E.; Hahn, F. E.; Raymond, K. N. *J. Am. Chem. Soc.* **1991**, *113*, 2965.
(8) Raymond, K. N.; McMurry, T. J.; Garrett, T. M. *Pure Appl. Chem.* **1988**, *60*, 545.
(9) McDermott, A. E.; Yachandra, V. K.; Guiles, R. D.; Cole, J. T.; Dexheimer, S. L.; Britt, R. D.; Sauer, K.; Klein, M. P. *Biochemistry* **1988**, *27*, 4021.
(10) Worland, S. T.; Yamagishi, H.; Isaacs, S.; Sauer, K.; Hearst, J. E. *Proc. Natl. Acad. Sci. U.S.A.* **1987**, *84*, 1774.
(11) Feher, G.; Isaacson, R. A.; McElroy, J. D.; Ackerson, I. E.; Okamura, M. Y. *Biochem. Biophys. Acta* **1974**, *368*, 135.
(12) Govindjee, Ed. *Bioenergetics of Photosynthesis*; Academic Press: New York, 1974.
(13) Morton, R. A. *Biochemistry of Quinones*; Academic Press: New York, 1965.
(14) Ruzicka, F. J.; Beinert, H.; Schepler, K. L.; Dunham, W. R.; Sands, R. H. *Proc. Natl. Acad. Sci. U.S.A.* **1975**, *72*, 2886.

0020-1669/92/1331-1001$03.00/0

to quinone or various carboxylic acids by breaking aromatic carbon–carbon bonds.[15,16]

Of more fundamental interest, perhaps, is the charge distribution in metal quinone systems.[17] The localized quinonoid (quinone, semiquinone, or catechol) electronic levels in metal complexes are close in energy to the metal electronic levels. The ordering of these levels affects the oxidation state of the metal and the quinone via the intramolecular transport scheme

$$M^{n-1}(Q^0) \leftarrow M^n(SQ^-) \rightarrow M^{n+1}(Cat^{2-})$$

where Q = quinone, SQ = semiquinonate, and Cat = catecholate. Studies have shown that this intramolecular charge distribution can be modified by several factors: (i) the donor ability of the counterligand, as in the compounds $Cu^{II}(DBCat)(bpy)$ and $Cu^{I}(DBSQ)(diphos)$,[18] (ii) the net charge on the complex, as in the $Mn^{II}(DBSQ)_2/[Mn^{III}(DBCat)_2]^-$ and $V^{III}(DBSQ)_3/[V^{IV}(DBCat)_3]^-$ systems,[19,20] (iii) variations in temperature, which affect the equilibrium in the system $Mn^{II}(DBSQ)_2(py)_2/Mn^{IV}(DBCat)_2(py)_2$[21] and (iv) the periodic dependence of metal valence orbital energies, as seen in the series $M^{II}(DBSQ)_2$ (M = Mn,[21] Co,[22] Ni,[22] Cu[23]) and $M^{III}(DBSQ)_3$ (M = V,[24] Cr,[25] Fe[26]). A good illustration of this last point is the comparison of the structures of $Mn^{II}_4(DBSQ)_8$[21] and $Fe^{III}_4(DBSQ)_4(DBCat)_4$[26] which are superficially isostructural and contain isoelectronic (d^5) metal ions. X-ray crystallography has been a valuable tool in evaluating charge distribution in metal quinone complexes, since differences in M–O, C–O, and OC–CO distances allow distinctions to be made between quinone, semiquinonate, and catecholate forms of complexation.[27] Structural determinations have been performed for semiquinonate and catecholate compounds with all first-row transition metals. Particularly relevant to the current investigation are the structures of the manganese compounds $Mn_4(DBSQ)_8$,[21] $Mn(DBCat)_2(py)_2$,[21] $Mn(DBCat)_3^{2-}$,[28] and $[Mn_2(Br_4Cat)_4(OPPh_3)]^{2-}$[19] and the iron compounds $Fe_4(DBSQ)_4(DBCat)_4$,[26] $Fe(DBSQ)_3$,[26] $Fe(DBCat)_3^{3-}$,[29] and $Fe(PhenSQ)_3 \cdot PhenQ$.[30] No neutral compounds are known for manganese or iron in which a metal in a low oxidation state is bound only to catecholate and donor ligands.

Interest in catecholate complexes in this laboratory stems from recent investigations of the synthesis of neutral manganese(II), iron(II), and cobalt(II) alkoxides and aryloxides by the alcoholysis of the amides $M[N(SiMe_3)_2]_2$ (M = Mn, Fe, Co).[31] It was found that the alcoholysis of the metal bis(trimethylsilyl)amides is a clean, high-yield, facile route to a variety of low-coordinate transition metal alkoxides. This led to the expectation that neutral manganese(II) and iron(II) catecholates could also be synthesized by this route. Earlier efforts along these lines, beginning with the reaction of cobalt bis(trimethylsilyl)amide with $DBCatH_2$, which resulted in the tetramer $[Co_4(DBCat)_4(THF)_{5.5}]$,[32] confirmed this view. In this paper, the synthesis and structures of the first neutral Mn(II) and Fe(II) catecholates, the dimers $Mn_2(DBCat)_2(py)_6$ and $Fe_2(DBCat)_2(py)_n$ (n = 4, 6), the tetramers $M_4(DBCat)_4(py)_6$ (M = Mn, Fe), and the first mixed-oxidation-state catecholate complex, the oxidation product $Mn_3(DBCat)_4(py)_4$, and some of their spectroscopic properties are reported.

Experimental Section

General Procedures. All reactions were performed under N_2 by using either modified Schlenk techniques or a Vacuum Atmospheres HE 43-2 drybox. Hexane and toluene were freshly distilled from Na/K and degassed three times before use. Pyridine was distilled from KOH pellets and stored over molecular sieves. 3,5-Di-*tert*-butylcatechol and 3,5-di-*tert*-butyl-*o*-benzoquinone were purchased from common sources and used as received. $Mn[N(SiMe_3)_2]_2$[33] and $Fe[N(SiMe_3)_2]_2$[34] were prepared by published procedures. ^1H NMR spectra were recorded in toluene-d_8 and pyridine-d_5 at 300 MHz on a GE QE-300 spectrometer and are referenced to the residual solvent peak. Infrared spectra were recorded in the range 4000–200 cm^{-1} as Nujol mulls between CsI plates using a Perkin-Elmer PE-1430 spectrometer. UV–visible spectra were recorded on a Hitachi U-2000 spectrometer. EPR spectra were obtained on a Bruker ER-200D spectrometer operating at 9.48 GHz.

$[Mn_2(3,5\text{-}t\text{-}Bu_2C_6H_2O_2)_2(py)_6]$ (1). A 0.667-g (3.0-mmol) sample of 3,5-di-*tert*-butylcatechol was dissolved in 25 mL of pyridine. A 1.13-g (3.0-mmol) amount of $Mn[N(SiMe_3)_2]_2$ was added slowly via a solids-addition funnel. The bright yellow solution was then allowed to stir for 1 h. Yellow crystals of **1** were obtained after filtration and reduction of volume to ca. 15 mL. X-ray-quality crystals were obtained by warming this solution until the crystals dissolved (>90 °C) and then cooling slowly to room temperature: yield 1.24 g, 81%; mp >290 °C dec.

$[Mn_4(3,5\text{-}t\text{-}Bu_2C_6H_2O_2)_4(py)_6]$ (2). Method 1. A 3.075-g (3.0-mmol) sample of **1** was dissolved with heating in toluene (15 mL). Upon slow cooling to room temperature, **2** was obtained in a yield of 80% (1.89 g).

Method 2. A 0.889-g (4.0-mmol) sample of 3,5-di-*tert*-butylcatechol was dissolved in hexane (50 mL). A 1.50-g (4.0-mmol) quantity of $Mn[N(SiMe_3)_2]_2$ was added via the solids-addition funnel, forming a colorless solution. After 90 min of stirring, 0.65 mL (8.0 mmol) of degassed pyridine was added via syringe, and a yellow precipitate formed immediately. The solution was heated until the precipitate dissolved, and the mixture was then filtered. Upon slow cooling to room temperature, **2** was obtained in 85% yield: mp >300 °C dec.

$[Mn_3(3,5\text{-}t\text{-}Bu_2C_6H_2O_2)_4(py)_4]$ (3). Compound **3** was first isolated from a solution of **2** that had been gradually exposed to air over 1 month. Subsequently, the following synthesis was found to produce an identical result: A 0.667-g (3.0-mmol) sample of 3,5-di-*tert*-butylcatechol was dissolved in toluene (50 mL). A 1.13-g (3.0-mmol) quantity of $Mn[N(SiMe_3)_2]_2$ was added via the solids-addition funnel, to form a colorless solution. After 90 min of stirring, 0.220 g (1.0 mmol) of 3,5-di-*tert*-butyl-*o*-benzoquinone dissolved in toluene (10 mL) was added via cannula, to give a green-brown solution. This was allowed to stir for 30 min and filtered. A 0.49-mL (6.0-mmol) portion of degassed pyridine was added via syringe, yielding a red-brown solution. From this solution, **3** was obtained on standing at room temperature overnight: yield 1.05 g, 77%; mp >250 °C dec.

$[Fe_2(3,5\text{-}t\text{-}Bu_2C_6H_2O_2)_2(py)_6]$ (4a) and $[Fe_2(3,5\text{-}t\text{-}Bu_2C_6H_2O_2)_2(py)_4]$ (4b). Black-red crystals of **4** were obtained in 85% yield in a manner identical to that used for **1**: mp (color change) 137–147 °C, dec >270 °C.

$[Fe_4(3,5\text{-}t\text{-}Bu_2C_6H_2O_2)_4(py)_6]$ (5). Orange crystals of **5** were obtained in ca. 70% yield by method 2 for compound **2**. Attempts to obtain **5** by dissolving **4** in toluene produced no change in **4**: mp (color change) >147 °C, dec >270 °C.

X-ray Crystallographic Studies. X-ray data for **1–5** were collected with a Syntex $P2_1$ diffractometer equipped with a locally modified LT-1 low-temperature device. Calculations were carried out on a Data General Eclipse computer using the SHELXTL, version 5, program system. Scat-

(15) Que, L., Jr. *Adv. Inorg. Biochem.* **1983**, *5*, 167.
(16) Que, L., Jr.; Kolanczyk, R. C.; White, L. S. *J. Am. Chem. Soc.* **1987**, *109*, 5373. Cox, D. A.; Que, L., Jr. *J. Am. Chem. Soc.* **1990**, *112*, 8085.
(17) Bhattacharya, S.; Boone, S. R.; Fox, G. A.; Pierpont, C. G. *J. Am. Chem. Soc.* **1990**, *112*, 1088.
(18) Buchanan, R. M.; Wilson-Blumenberg, C.; Trapp, C.; Larsen, S. K.; Greene, D. L.; Pierpont, C. G. *Inorg. Chem.* **1986**, *25*, 3070.
(19) Larsen, S. K.; Pierpont, C. G.; DeMunno, G.; Dolcetti, G. *Inorg. Chem.* **1986**, *25*, 4828.
(20) Cass, M. E.; Gordon, N. R.; Pierpont, C. G. *Inorg. Chem.* **1986**, *25*, 3962.
(21) Lynch, M. W.; Hendrickson, D. N.; Fitzgerald, B. J.; Pierpont, C. G. *J. Am. Chem. Soc.* **1984**, *106*, 2041.
(22) Buchanan, R. M.; Fitzgerald, B. J.; Pierpont, C. G. *Inorg. Chem.* **1979**, *18*, 3439.
(23) Kahn, O.; Prins, R.; Reedijk, J.; Thompson, J. S. *Inorg. Chem.* **1987**, *26*, 3557.
(24) Cass, M. E.; Greene, D. L.; Buchanan, R. M.; Pierpont, C. G. *J. Am. Chem. Soc.* **1983**, *105*, 2680.
(25) Sofen, S. R.; Ware, D. C.; Cooper, S. R.; Raymond, K. N. *Inorg. Chem.* **1979**, *18*, 234.
(26) Boone, S. R.; Purser, G. H.; Chang, H.-R.; Lowery, M. D.; Hendrickson, D. N.; Pierpont, C. G. *J. Am. Chem. Soc.* **1989**, *111*, 2292.
(27) Pierpont, C. G.; Buchanan, R. M. *Coord. Chem. Rev.* **1981**, *38*, 45.
(28) Hartman, J. A. R.; Foxman, B. M.; Cooper, S. R. *J. Chem. Soc., Chem. Commun.* **1982**, 583.
(29) Raymond, K. N.; Isied, S. S.; Brown, L. D.; Fronczek, F. R.; Nibert, J. H. *J. Am. Chem. Soc.* **1976**, *98*, 1767.
(30) Buchanan, R. M.; Kessel, S. L.; Downs, H. H.; Pierpont, C. G.; Hendrickson, D. N. *J. Am. Chem. Soc.* **1978**, *100*, 7894.
(31) Bartlett, R. A.; Ellison, J. J.; Power, P. P.; Shoner, S. C. *Inorg. Chem.* **1991**, *30*, 2888. Sigel, G. A.; Bartlett, R. A.; Decker, D.; Olmstead, M. M.; Power, P. P. *Inorg. Chem.* **1987**, *26*, 1773.
(32) Olmstead, M. M.; Power, P. P.; Sigel, G. A. *Inorg. Chem.* **1988**, *27*, 580.
(33) Bürger, H.; Wannagat, U. *Monatsh. Chem.* **1964**, *95*, 1099.
(34) Andersen, R. A.; Faegri, K.; Green, J. C.; Haaland, A.; Lappert, M. F.; Leung, W.-P. *Inorg. Chem.* **1988**, *27*, 1782.

Table I. Abridged Summary of Data Collection, Structure Solution, and Refinement for **1–5**

	1	**2**	**3**	**4**	**5**
formula	$C_{58}H_{70}N_6O_4Mn_2$	$C_{86}H_{110}N_6O_8Mn_4$	$C_{76}H_{100}N_4O_8Mn_3$	$C_{106}H_{130}N_{10}O_8Fe_4$	$C_{86}H_{110}N_6O_8Fe_4$
fw	1025.11	1575.62	1362.48	1895.66	1579.25
cryst syst	triclinic *P*	orthorhombic *P*	monoclinic *P*	triclinic *P*	triclinic *P*
a, Å	13.049 (4)	15.802 (4)	17.184 (5)	13.559 (4)	14.868 (4)
b, Å	13.531 (4)	22.990 (4)	19.184 (5)	15.410 (5)	16.157 (7)
c, Å	19.107 (5)	27.825 (7)	25.239 (6)	16.594 (5)	20.309 (6)
α, deg	90.30 (2)			62.70 (2)	67.47 (3)
β, deg	101.35 (2)		95.32 (2)	75.95 (2)	88.15 (2)
γ, deg	106.37 (2)			80.27 (2)	76.59 (3)
V, Å^3	3167 (1)	10109 (4)	8284 (4)	2957 (1)	4375 (3)
space group	$P\bar{1}$	*Pbcb*	$P2_1/n$	$P\bar{1}$	$P\bar{1}$
Z	2	4	4	1	2
D(calc), g/cm^3	1.24	1.13	1.16	1.24	1.25
linear abs coeff, cm^{-1}	4.41	5.21	4.79	5.52	7.02
2θ range, deg	0–47	0–50	0–50	0–50	0–50
no. of obs reflns [$I > 2\sigma(I)$]	7089	5669	7780	5160	9803
no. of variables	775	562	908	681	1033
R, R_w	0.048, 0.053	0.073, 0.076	0.084, 0.086	0.080, 0.065	0.068, 0.070

tering factors were from common sources, and an absorption correction was applied using the method described in ref 35.

X-ray-quality crystals of the title compounds were grown from concentrated solutions in pyridine (**1** and **4**), toluene (**2**), or hexane (**3** and **5**). Crystals of **1–5** were removed from the Schlenk tube under a stream of N_2 and immediately covered with a layer of hydrocarbon oil. A suitable crystal was selected, attached with grease to a glass fiber, and immediately placed in the low-temperature nitrogen stream. Some details of the data collection and refinement are given in Table I. Further details are provided in the supplementary material. The structures of **2**, **3**, and **5** were solved by direct methods and subsequently refined by blocked cascade least-squares refinement. In the cases of **1** and **4**, the metal atom positions were obtained from a Patterson map, and other non-hydrogen atoms were located in subsequent difference maps. In all cases, hydrogen atoms were included by use of a riding model with C–H distances of 0.96 Å and isotropic thermal parameters equal to 1.2 times that of the bonded carbon. All non-hydrogen atoms were refined anisotropically. Fractional coordinates for important atoms in **1–5** are given in Table II, and selected bond distances and angles, in Table III.

Spectroscopic Data. The UV–visible absorption spectra of **1** and **2** in pyridine and toluene were essentially featureless, with a gradual rise in intensity toward higher wavenumber. The UV–visible data for **3–5** in the indicated solvent were as follows: **3** (toluene), 26 300 cm^{-1} (ϵ = 5200 M^{-1} cm^{-1}); **4** (pyridine), 20 200 cm^{-1} (ϵ = 5600 M^{-1} cm^{-1}); **5** (toluene), 23 100 cm^{-1} (ϵ = 3900 M^{-1} cm^{-1}). Selected IR data were as follows (in cm^{-1}). **1**: ν_{C-O} 1316 (br) (m), 1255 (br) (m), 1232 (br) (m), 1211 (m); ν_{M-O} and ν_{M-N} 618 (m), 579 (br) (w), 532 (br) (w), 518 (br) (w), 432 (br) (w), 410 (br) (w), 370 (br) (w). **2**: ν_{C-O} 1310 (br) (s), 1258 (br) (s), 1237 (br) (s), 1198 (m); ν_{M-O} and ν_{M-N} 619 (w), 578 (br) (w), 539 (br) (w), 519 (br) (w), 481 (br) (w), 459 (w), 438 9br) (w), 423 (br) (w), 411 (w), 355 (vbr) (w), 323 (br) (w). **3**: ν_{C-O} 1311 (br) (m), 1270 (m), 1258 (m), 1235 (br) (s), 1212 (sh) (m), 1198 (m); ν_{M-O} and ν_{M-N} 623 (br) (w), 608 (br) (w), 570 (br) (w), 545 (br) (w), 534 (br) (w), 510 (br) (w), 452 (br) (w), 452 (br) (w), 410 (w), 392 (br) (w), 300 (br) (w). **4**: ν_{C-O} 1318 (br) (m), 1252 (br) (m), 1230 (br) (m), 1210 (br) (w); ν_{M-O} and ν_{M-N} 615 (sh) (w), 592 (br) (w), 551 (br) (w), 442 (br) (w), 415 (br) (w), 381 (br) (w). **5**: ν_{C-O} 1309 (br) (s), 1258 (br) (s), 1227 (s), 1216 (s), 1198 (br) (m); ν_{M-O} and ν_{M-N} 618 (br) (w), 606 (br) (w), 587 (br) (w), 542 (br) (w), 485 (br) (w), 460 (br) (w), 440 (br) (w), 418 (w), 390 (br) (w), 372 (br) (w), 324 (br) (w), 276 (sh) (w). ^{1}H NMR spectra for **1–3** showed no isotropically shifted peaks, presumably due to paramagnetic broadening. ^{1}H NMR spectra for **4** and **5** gave the following shifts (in ppm) and intensities: **4** (C_5D_5N), 24.41 (1 H), 9.13 (12 H), 7.55 (12 H), 7.23 (13 H), 6.57 (9 H), 4.89 (2 H), 2.12 (1 H); **5** (C_7D_8), 18.31 (9 H), 7.10 (2 H), 1.24 (2 H), 0.886 (3 H), −0.749 (9 H).

EPR spectra were recorded at ca. 10 K for frozen 2 mM solutions of **1–5**. The spectrum of compound **1** in pyridine gave a multiline signal centered at g = 1.98 with a ^{55}Mn ($I = {}^5/_2$) hyperfine coupling constant of 87.5 G, which is characteristic of Mn in a +2 oxidation state. The spectrum also contains an intense, broad resonance at g = 2.48 and several other broad resonances at g = 1.49, 2.98, 3.67, and 12.93. The spectrum of **2** in toluene contained one large broad signal at g = 1.97 with no hyperfine coupling and one smaller resonance at g = 3.03. No spectrum was observed for compound **3** in toluene over the range 5–30 K. Compound **4** gives only one narrow peak in pyridine at g = 5.48. The spectrum of **5** in toluene contains one broad signal at g = 13.91.

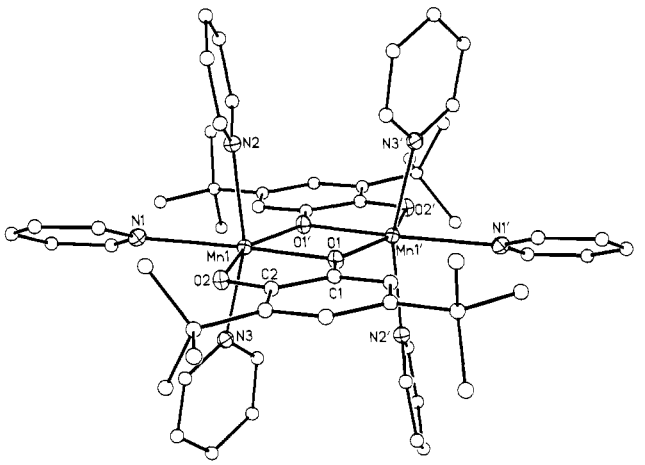

Figure 1. Computer-generated plot of the structure of **1**. Manganese, oxygen, and nitrogen are shown as 30% probability thermal ellipsoids, and carbon atoms are shown as spheres of arbitrary radius. H atoms have been omitted for clarity.

Results and Discussion

Structural Descriptions. [Mn_2(3,5-*t*-$Bu_2C_6H_2O_2$)$_2$(py)$_6$] (1). The structure of **1** is shown in Figure 1. Each unit cell contains two centrosymmetric dimers of **1**, with the result that the asymmetric unit possesses two crystallographically independent, but chemically identical, halves of the dimers. The dimers are composed of two six-coordinate manganese atoms bridged by oxygens from two catecholates. The metals are further coordinated to a terminal oxygen from a catecholate and three pyridines. The catecholate ring planes are coplanar with one coordinated pyridine of each manganese, and the remaining four pyridine rings are perpendicular to this plane. The bridging Mn–O distances are asymmetric (2.172 (2) vs 2.096 (2) Å) and slightly longer than the terminal Mn–O distances (2.083 (2) Å). The O–C distances for bridging (br) and terminal (t) oxygen are very similar to each other (C–O(br) = 1.358 (3) Å, C–O(t) = 1.339 (4) Å). The bridging oxygens are planar, with rather narrow Mn–O(br)–Mn angles of 103.2 (1)° and asymmetric Mn–O–C angles (111.8 (2) vs 144.8 (2)°). The terminal Mn–O–C angle is 115.2 (2)°. The Mn–N bond lengths for the pyridines that are coplanar and perpendicular to the catecholate plane are 2.411 (3) and 2.306 (3) Å, respectively. The geometry at the metal in **1** is quite distorted from typical octahedral geometry. The angles at manganese vary from 76.8 (1) to 119.1 (1)°.

[Mn_4(3,5-*t*-$Bu_2C_6H_2O_2$)$_4$(py)$_6$] (2). Compound **2** is illustrated in Figure 2. The molecules have a crystallographically imposed

(35) *International Tables for X-Ray Crystallography*; Kynoch Press: Birmingham, U.K., 1974; Vol. IV. The absorption correction was made using the program XABS, which obtains an absorption tensor from $F_o - F_c$ differences: Moezzi, B. Ph.D. Dissertation, University of California, Davis, 1987.

Table II. Selected Atomic Coordinates ($\times 10^4$) and Isotropic Thermal Parameters ($Å^2 \times 10^3$) for **1–5**

	x	y	z	U^a		x	y	z	U^a
				Compound **1**					
Mn(1)	5142 (1)	4257 (1)	4344 (1)	19 (1)	N(3)	6112 (2)	3285 (2)	5007 (1)	24 (1)
Mn(2)	−294 (1)	5709 (1)	610 (1)	21 (1)	N(4)	−22 (2)	4660 (2)	1553 (1)	25 (1)
O(1)	3992 (2)	4416 (2)	4988 (1)	22 (1)	N(5)	−1184 (2)	6632 (2)	−173 (1)	28 (1)
O(2)	3804 (2)	2978 (2)	3974 (1)	22 (1)	N(6)	−1307 (2)	6206 (2)	1418 (2)	30 (1)
O(3)	1031 (2)	5609 (2)	108 (1)	24 (1)	C(1)	3011 (3)	3690 (2)	4785 (2)	20 (1)
O(4)	959 (2)	7032 (2)	1048 (1)	24 (1)	C(2)	2928 (3)	2920 (2)	4254 (2)	20 (1)
N(1)	5967 (2)	3725 (2)	3440 (1)	26 (1)	C(15)	1952 (3)	6385 (2)	340 (2)	21 (1)
N(2)	4611 (2)	5239 (2)	3438 (1)	26 (1)	C(16)	1903 (3)	7149 (2)	837 (2)	20 (1)
				Compound **2**					
Mn(1)	−323 (1)	7047 (1)	−699 (1)	20 (1)	N(2)	1789 (3)	6823 (2)	893 (2)	33 (2)
Mn(2)	7519 (1)	6886 (1)	334 (1)	21 (1)	N(3)	924 (3)	5900 (2)	267 (2)	26 (2)
O(1)	−549 (2)	6817 (2)	12 (1)	23 (1)	C(1)	−1139 (4)	6701 (2)	346 (2)	19 (2)
O(2)	−131 (2)	7063 (2)	903 (1)	22 (1)	C(2)	−897 (4)	6795 (2)	833 (2)	22 (2)
O(3)	973 (2)	7132 (2)	−393 (1)	21 (1)	C(15)	1528 (4)	6829 (2)	−680 (2)	23 (2)
O(4)	357 (2)	6544 (2)	−1158 (1)	25 (1)	C(16)	1199 (4)	6525 (2)	−1078 (2)	22 (2)
N(1)	−1572 (3)	6823 (2)	−1022 (2)	27 (2)					
				Compound **3**					
Mn(1)	9637 (1)	3386 (1)	3672 (1)	18 (1)	N(2)	8714 (4)	5735 (4)	2908 (3)	23 (2)
Mn(2)	8607 (1)	4652 (1)	3245 (1)	16 (1)	N(3)	8549 (4)	5046 (4)	4074 (3)	20 (2)
Mn(3)	7500 (1)	4125 (1)	2256 (1)	15 (1)	N(4)	7418 (4)	5022 (4)	1701 (3)	23 (2)
O(1)	8544 (3)	3545 (3)	3563 (2)	19 (2)	C(1)	8168 (4)	3223 (4)	3958 (3)	17 (2)
O(2)	9439 (3)	2994 (3)	4334 (2)	25 (2)	C(2)	8666 (4)	2955 (4)	4386 (3)	18 (3)
O(3)	9795 (3)	4318 (3)	3398 (2)	18 (2)	C(15)	10586 (4)	4469 (4)	3434 (3)	16 (2)
O(4)	10714 (3)	3314 (3)	3748 (2)	25 (2)	C(16)	11076 (4)	3919 (5)	3622 (3)	20 (3)
O(5)	8587 (3)	4199 (3)	2452 (2)	17 (2)	C(29)	9005 (4)	3862 (4)	2095 (3)	16 (2)
O(6)	7766 (3)	3493 (3)	1739 (2)	20 (2)	C(30)	8553 (4)	3509 (4)	1686 (3)	16 (2)
O(7)	7396 (3)	4610 (3)	2906 (2)	16 (2)	C(43)	6616 (4)	4646 (4)	3002 (3)	16 (2)
O(8)	6430 (3)	3942 (3)	2244 (2)	19 (2)	C(44)	6100 (4)	4302	2631 (3)	15 (2)
N(1)	9561 (4)	2496 (4)	3149 (3)	20 (2)					
				Compound **4**					
Fe(1)	4231 (1)	4456 (1)	997 (1)	20 (1)	N(3)	4976 (5)	2997 (4)	1139 (4)	29 (3)
Fe(2)	90 (1)	9285 (1)	5218 (1)	19 (1)	N(4)	1236 (4)	8511 (4)	6608 (4)	20 (3)
O(1)	5751 (4)	5146 (4)	343 (3)	21 (3)	N(5)	2544 (4)	9799 (4)	4596 (4)	25 (3)
O(2)	4683 (4)	4319 (4)	2097 (3)	21 (2)	C(1)	6173 (5)	5077 (5)	1012 (5)	20 (4)
O(3)	−324 (4)	9473 (3)	4727 (3)	21 (3)	C(2)	5600 (5)	4658 (5)	1951 (5)	17 (3)
O(4)	1179 (5)	8139 (3)	4947 (3)	19 (2)	C(30)	−353 (5)	8771 (5)	4451 (5)	19 (4)
N(1)	2766 (4)	3271 (5)	1940 (4)	27 (3)	C(31)	468 (5)	8066 (5)	4561 (5)	16 (3)
N(2)	3342 (4)	5850 (4)	943 (4)	23 (3)					
				Compound **5**					
Fe(1)	2629 (1)	4547 (1)	8101 (1)	15 (1)	N(2)	−414 (3)	4182 (3)	7304 (3)	16 (2)
Fe(2)	970 (1)	4396 (1)	7175 (1)	15 (1)	N(3)	4259 (3)	4317 (4)	6415 (3)	20 (2)
Fe(3)	2949 (1)	3960 (1)	6697 (1)	15 (1)	N(4)	2255 (3)	4856 (4)	5590 (3)	23 (2)
Fe(4)	2361 (1)	2578 (1)	8362 (1)	15 (1)	N(5)	3211 (3)	2126 (4)	9389 (3)	22 (2)
O(1)	2287 (3)	5018 (3)	7013 (2)	16 (2)	N(6)	2791 (3)	1146 (3)	8468 (3)	21 (2)
O(2)	482 (3)	5682 (3)	6619 (2)	22 (2)	C(1)	1985 (4)	5942 (4)	6607 (3)	17 (2)
O(3)	1483 (3)	4044 (3)	8222 (2)	15 (2)	C(2)	1025 (4)	6285 (4)	6409 (3)	17 (2)
O(4)	1271 (3)	2347 (3)	8916 (2)	21 (2)	C(15)	784 (4)	3931 (4)	8690 (3)	15 (2)
O(5)	3311 (3)	3328 (3)	7845 (2)	16 (2)	C(16)	691 (4)	3022 (4)	9063 (3)	16 (2)
O(6)	3865 (3)	4248 (3)	8531 (2)	21 (2)	C(29)	4232 (4)	3073 (4)	8090 (3)	14 (2)
O(7)	1781 (3)	3217 (3)	7197 (2)	17 (2)	C(30)	4497 (4)	3551 (4)	8467 (3)	16 (2)
O(8)	3239 (3)	2894 (3)	6432 (2)	19 (2)	C(43)	1813 (4)	2575 (4)	6899 (3)	15 (2)
N(1)	2261 (3)	5835 (3)	8240 (3)	19 (2)	C(44)	2595 (4)	2413 (4)	6499 (3)	17 (2)

[a] Equivalent isotropic U defined as one-third of the trace of the orthogonalized U_{ij} tensor.

2-fold axis perpendicular to the Mn(2)–O(3)–Mn(2′)–O(3′) plane. The four manganese atoms are bridged by four catecholate ligands. Two of the catecholates have one μ^3-bridging and one terminal oxygen; the other two catecholates have two μ^2-bridging oxygens. In both cases, each catecholate connects three metal atoms such that two of the manganese atoms are five-coordinate and bonded to one terminal oxygen, two μ^2-bridging oxygens, one μ^3-bridging oxygen, and one pyridine. The remaining manganese atoms are six-coordinate and bound to two μ^2-bridging oxygens, two μ^3-bridging oxygens, and two pyridines. The result of this coordination gives the core of the molecule a basket-like appearance, with the μ^3-bridging oxygens and six-coordinate manganese atoms forming the base and the four μ^2-bridging oxygens and five-coordinate manganese atoms forming the rim. The five-coordinate manganese atoms have distorted trigonal bipyramidal geometry. The two μ^2-bridging oxygens and the terminal oxygen comprise the equatorial atoms of the bipyramid, while the μ^3-bridging oxygen and the pyridine occupy the axial positions. The Mn–O bond lengths involving the two μ^2-bridging oxygens are unequal (2.077 (4) and 2.144 (4) Å) and substantially longer than the terminal Mn–O bond of 2.032 (4) Å. The triply bridging Mn–O distance is much longer (2.227 (4) Å) and is essentially the same length as the Mn–N bond distance (2.229 (5) Å) trans to it. The two six-coordinate manganese atoms possess extremely distorted octahedral geometry. The angles at the Mn atoms vary from 73.4 (1) to 123.3 (2)°. The metal–oxygen bond distances fall in the range 2.129 (4)–2.289 (4) Å and depend upon the trans ligand and the degree of bridging by the oxygen. Two of the μ^2-bridging oxygens are planar ($\sum°O = 359.5°$) with very different Mn–O distances (2.077 (4) vs 2.246 (4) Å) and O–C distances similar to those for the terminal oxygens (1.343 (7) vs 1.349 (7) Å). In contrast, the remaining μ^2-bridging oxygens are pyramidal ($\sum°O = 312.4°$) and have two very similar Mn–O distances (2.144 (4) and 2.148 (4) Å). Their O–C distances are almost identical to

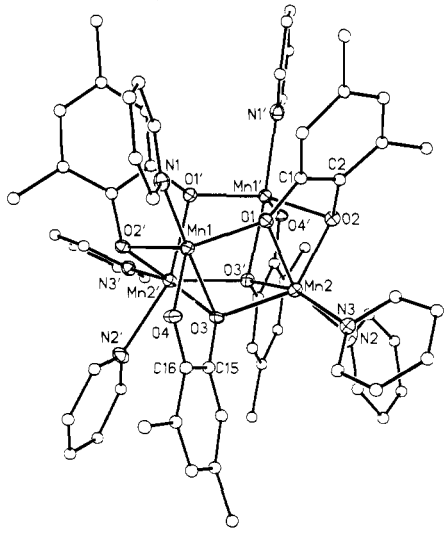

Figure 2. Computer-generated plot of the structure of **2**. Manganese, oxygen, and nitrogen are shown as 30% probability thermal ellipsoids, and carbon atoms are shown as spheres of arbitrary radius. H atoms and *tert*-butyl methyls have been omitted for clarity.

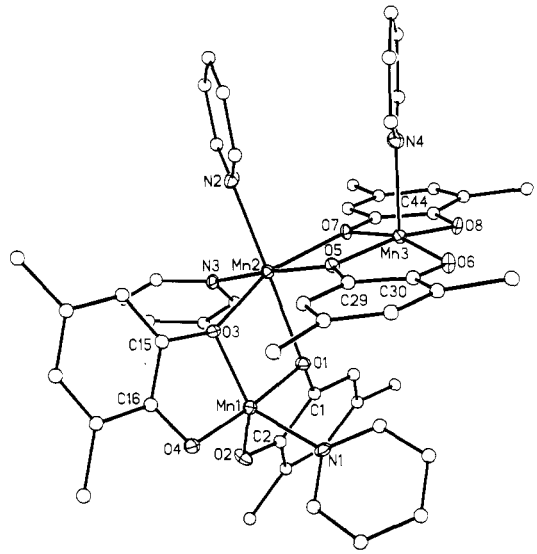

Figure 3. Computer-generated plot of the structure of **3**. Manganese, oxygen, and nitrogen are shown as 30% probability thermal ellipsoids, and carbon atoms are shown as spheres of arbitrary radius. H atoms and *tert*-butyl methyls have been omitted for clarity.

those found for the μ^3-bridging oxygens (1.373 (7) vs 1.376 (7) Å). The μ^3-bridging oxygens have two long (2.227 (4) and 2.289 (4) Å) and one shorter (2.129 (4) Å) Mn–O distance. The oxygens have distorted tetrahedral coordination angles that vary from 96.3 to 119.9°.

$[Mn_3(3,5\text{-}t\text{-}Bu_2C_6H_2O_2)_4(py)_4]$ (3). Compound **3** is illustrated in Figure 3. This structure contains two five-coordinate manganese(III) atoms, each of which is linked to a central six-coordinate manganese(II) by two μ^2-bridging catecholate oxygens. The two Mn_2O_2 bridging moieties are planar, and the angle between the planes is 94.6°. Two cis-pyridine ligands complete the octahedral coordination sphere at the central manganese(II). The angles at Mn(II) vary from 72.0 (2) to 104.8 (2)°. The Mn(II)–O distances vary from 2.142 (5) to 2.277 (6) Å, and the Mn–N bonds are 2.235 (7) and 2.259 (7) Å. The two Mn(III) ions have very different geometries. Mn(1) has trigonal bipyramidal geometry. One bridging oxygen, a terminal oxygen, and a coordinated pyridine form the equatorial plane ($\sum°$Mn(1) = 359.8°), while the remaining terminal and bridging oxygens comprise the axial positions. In contrast, Mn(3) has a square pyramidal configuration. The oxygens from the two catechol ligands chelating Mn(3) form the planar square base of the pyramid (average

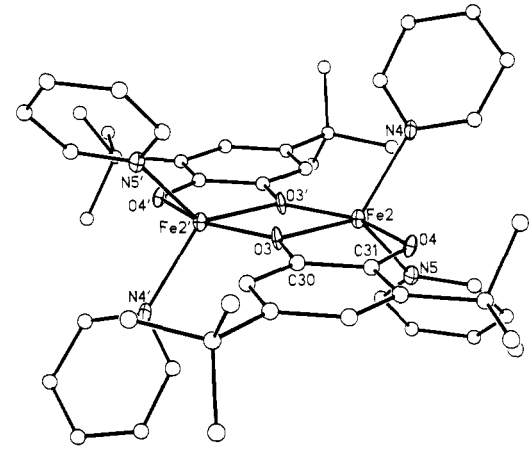

Figure 4. Computer-generated plot of the structure of **4b**. Iron, oxygen, and nitrogen are shown as 30% probability thermal ellipsoids, and carbon atoms are shown as spheres of arbitrary radius. H atoms have been omitted for clarity.

deviation = 0.087 Å), with the metal displaced 0.175 Å toward the apical pyridine. The square plane of oxygens is distorted, with angles at Mn(3) ranging from 84.7 (2) to 99.9 (2)°. The O–Mn–N angles average 96.8 (2)°, and the Mn–N distance is longer for Mn(3) than for Mn(1) (2.216 (7) vs 2.157 (7) Å). The Mn–O distances are similar for both metals, and the bridging distances (1.911 (5) Å (av)) are slightly longer than the terminal distances (1.869 (6) Å (av)) in both cases. Three of the bridging oxygens have planar coordination, while the coordination of the remaining bridging oxygen (O(1)) is somewhat pyramidal ($\sum°$O(1) = 342.6°). It has the longest bond to the central metal (2.277 (6) Å) and a very narrow M–O–M angle (97.0 (2)°). The O–C distances are shorter for the terminal oxygens, but all fall into the range of distances expected for catechol, rather than semiquinone, ligands.

$[Fe_2(3,5\text{-}t\text{-}Bu_2C_6H_2O_2)_2(py)_6]$ (4a) and $[Fe_2(3,5\text{-}t\text{-}Bu_2C_6H_2O_2)_2(py)_4]$ (4b). The unit cell is composed of two centrosymmetric dimers. One (**4a**) has a metal that is six-coordinate, as in **1**, and another (**4b**) has two pyridines coordinated to each iron, affording five-coordinate metals. The six-coordinate iron dimer is essentially isostructural with its manganese analogue **1**. Two differences are noteworthy. First, the doubly bridging M–O bond distances in the six-coordinate dimer of **4** are much more asymmetric (ΔFe–O = 0.224 Å for **4a**, ΔMn–O = 0.065 Å (av) for **1**), and second, the M–N distances are approximately equal, in contrast to those in **1**, which differ by ca. 0.1 Å. The five-coordinate dimer **4b** is shown in Figure 4. The briding is similar to that seen in the other six-coordinate dimers. The geometry at each metal is trigonal bipyramidal. The two pyridines and the chelating μ^2 oxygen form the equatorial plane ($\sum°$ = 360.0°). The terminal oxygen and the μ^2 oxygen from the other monomeric unit take up the axial positions (O–Fe–O = 157.2 (2)°). The bridging distances are more symmetric in this dimer (ΔFe–O = 0.078 Å); nonetheless, the angles at the bridging oxygens are similar to those seen for the six-coordinate dimers. The metal–nitrogen bonds are ca. 0.10 Å shorter in the five-coordinate dimer than in the six-coordinate one. The difference between the C–O(br) and C–O(t) distances in these dimers is negligible.

$[Fe_4(3,5\text{-}t\text{-}Bu_2C_6H_2O_2)_4(py)_6]$ (5). Compound **5** is depicted in Figure 5. In this case, each of the four iron atoms is bound to one terminal and three triply bridging oxygens, which gives the compound a Fe_4O_4 distorted cubane core. Fe(1) and Fe(2), which are each bound to one pyridine donor, have irregular trigonal bipyramidal geometry. Fe(3) and Fe(4), each bind two pyridines and have distorted octahedral metal coordination. For Fe(1) and Fe(2), the equatorial plane is formed from the terminal oxygen and two intermetallic bridging oxygens ($\sum°$Fe = 351.1°), while the triply bridging chelating oxygen and the pyridine occupy axial positions (O–Fe–N = 165.7 (2)° (av)). The octahedral geometry of Fe(3) and Fe(4) is quite distorted, with angles ranging from 74.7 (2) to 111.9 (2)°. For all four metals, the Fe–O bridging

Table III. Selected Bond Lengths (Å) and Angles (deg) for **1–5**

Compound **1**

Mn(1)···Mn(1′)	3.346 (1)	Mn(2)···Mn(2′)	3.346 (1)	Mn(1)–N(2)	2.306 (3)	Mn(1)–N(3)	2.293 (3)
Mn(1)–O(1)	2.172 (2)	Mn(1)–O(2)	2.083 (2)	O(1)–C(1)	1.358 (3)	O(2)–C(2)	1.339 (4)
Mn(1)–O(1′)	2.096 (2)	Mn(1)–N(1)	2.411 (3)	C(1)–C(2)	1.417 (5)		
O(1)–Mn(1)–O(2)	77.5 (1)	O(1)–Mn(1)–O(1′)	76.8 (1)	N(1)–Mn(1)–N(2)	80.9 (1)	N(3)–Mn(1)–O(1′)	91.7 (1)
O(2)–Mn(1)–O(1′)	154.3 (1)	O(1)–Mn(1)–N(1)	163.8 (1)	N(2)–Mn(1)–O(1′)	91.3 (1)	C(1)–O(1)–Mn(1′)	144.8 (2)
O(1)–Mn(1)–N(2)	96.3 (1)	O(1)–Mn(1)–N(3)	103.7 (1)	Mn(1)–O(1)–Mn(1′)	103.2 (1)	Mn(1)–O(2)–C(2)	115.2 (2)
O(2)–Mn(1)–N(1)	86.6 (1)	O(2)–Mn(1)–N(2)	93.0 (1)	Mn(1)–O(1)–C(1)	111.8 (2)	O(1)–C(1)–C(2)	117.2 (3)
O(2)–Mn(1)–N(3)	92.9 (1)	N(2)–Mn(1)–N(3)	159.9 (1)	O(2)–C(2)–C(1)	118.0 (2)		
N(1)–Mn(1)–N(3)	80.3 (1)	N(1)–Mn(1)–O(1′)	119.1 (1)				

Compound **2**

Mn(1)···Mn(2)	3.358 (2)	Mn(1)···Mn(2′)	3.150 (2)	Mn(2)–O(3)	2.129 (4)	Mn(2)–O(3′)	2.289 (4)
Mn(2)···Mn(2′)	3.380 (2)	Mn(1)···Mn(1′)	4.410 (2)	Mn(1)–N(1)	2.229 (5)	Mn(2)–N(2)	2.266 (5)
Mn(1)–O(1)	2.077 (4)	Mn(1)–O(3)	2.227 (4)	Mn(2)–N(3)	2.291 (5)	O(1)–C(1)	1.343 (7)
Mn(1)–O(4)	2.032 (4)	Mn(1)–O(2′)	2.144 (4)	O(2)–C(2)	1.373 (7)	O(3)–C(15)	1.376 (7)
Mn(2)–O(1)	2.246 (4)	Mn(2)–O(2)	2.148 (4)	C(1)–C(2)	1.426 (8)	O(4)–C(16)	1.349 (7)
				C(15)–C(16)	1.408 (8)		
O(1)–Mn(1)–O(2′)	121.3 (1)	O(1)–Mn(1)–O(3)	79.4 (1)	N(2)–Mn(2)–N(3)	84.6 (2)	N(2)–Mn(2)–O(3′)	84.4 (2)
O(1)–Mn(1)–O(4)	123.0 (2)	O(1)–Mn(1)–N(1)	99.9 (2)	N(3)–Mn(2)–O(3′)	164.3 (2)	Mn(1)–O(1)–Mn(2)	101.8 (2)
O(3)–Mn(1)–O(2′)	83.5 (1)	O(3)–Mn(1)–O(4)	78.7 (1)	Mn(1)–O(1)–C(1)	145.8 (3)	Mn(2)–O(1)–C(1)	111.9 (3)
O(3)–Mn(1)–N(1)	171.4 (2)	O(4)–Mn(1)–N(1)	94.8 (2)	Mn(1′)–O(2)–Mn(2)	94.4 (1)	Mn(2)–O(2)–C(2)	112.5 (3)
O(4)–Mn(1)–O(2′)	107.5 (1)	N(1)–Mn(1)–O(2′)	103.9 (2)	Mn(1′)–O(2)–C(2)	105.5 (3)	Mn(1)–O(3)–Mn(2)	100.8 (1)
O(1)–Mn(2)–O(2)	73.4 (1)	O(1)–Mn(2)–O(3)	77.9 (1)	Mn(1)–O(3)–Mn(2′)	88.4 (1)	Mn(2)–O(3)–Mn(2′)	99.8 (1)
O(1)–Mn(2)–O(3′)	103.8 (1)	O(1)–Mn(2)–N(2)	158.7 (2)	Mn(1)–O(3)–C(15)	108.6 (3)	Mn(2)–O(3)–C(15)	121.4 (3)
O(1)–Mn(2)–N(3)	90.4 (2)	O(2)–Mn(2)–O(3)	139.1 (1)	Mn(2′)–O(3)–C(15)	129.7 (3)	Mn(1)–O(4)–C(16)	115.8 (3)
O(2)–Mn(2)–O(3′)	82.0 (1)	O(2)–Mn(2)–N(2)	88.6 (2)	O(1)–C(1)–C(2)	116.2 (5)	O(2)–C(2)–C(1)	116.0 (5)
O(2)–Mn(2)–N(3)	109.0 (2)	O(3)–Mn(2)–O(3′)	77.3 (1)	O(3)–C(15)–C(16)	118.2 (3)	O(4)–C(16)–C(15)	118.5 (5)
O(3)–Mn(2)–N(2)	123.3 (2)	O(3)–Mn(2)–N(3)	99.6 (2)				

Compound **3**

Mn(1)···Mn(2)	3.136 (3)	Mn(2)···Mn(3)	3.162 (3)	Mn(3)–O(8)	1.869 (5)	Mn(3)–N(4)	2.216 (7)
Mn(1)–O(1)	1.897 (5)	Mn(1)–O(2)	1.891 (6)	O(1)–C(1)	1.382 (10)	O(2)–C(2)	1.348 (9)
Mn(1)–O(3)	1.944 (6)	Mn(1)–O(4)	1.849 (5)	C(1)–C(2)	1.411 (11)	O(3)–C(15)	1.383 (9)
Mn(1)–N(1)	2.157 (7)	Mn(2)–O(1)	2.277 (6)	O(4)–C(16)	1.367 (10)	C(15)–C(16)	1.405 (11)
Mn(2)–O(3)	2.142 (5)	Mn(2)–O(5)	2.179 (5)	O(5)–C(29)	1.365 (9)	O(6)–C(30)	1.373 (9)
Mn(2)–O(7)	2.177 (5)	Mn(2)–N(2)	2.259 (7)	C(29)–C(30)	1.407 (10)	O(7)–C(43)	1.385 (8)
Mn(2)–N(3)	2.235 (7)	Mn(3)–O(5)	1.893 (5)	O(8)–C(44)	1.361 (10)	C(43)–C(44)	1.395 (10)
Mn(3)–O(6)	1.868 (6)	Mn(3)–O(7)	1.910 (5)				
O(1)–Mn(1)–O(2)	86.3 (2)	O(1)–Mn(1)–O(3)	88.3 (2)	O(6)–Mn(3)–O(8)	99.9 (2)	O(6)–Mn(3)–N(4)	93.9 (3)
O(1)–Mn(1)–O(4)	174.5 (3)	O(1)–Mn(1)–N(1)	92.0 (2)	O(7)–Mn(3)–O(8)	86.2 (2)	O(7)–Mn(3)–N(4)	99.2 (3)
O(2)–Mn(1)–O(3)	136.3 (3)	O(2)–Mn(1)–O(4)	98.0 (2)	O(8)–Mn(3)–N(4)	97.5 (2)	Mn(1)–O(1)–Mn(2)	97.0 (2)
O(2)–Mn(1)–N(1)	102.7 (3)	O(3)–Mn(1)–O(4)	86.2 (2)	Mn(1)–O(1)–C(1)	110.3 (4)	Mn(2)–O(1)–C(1)	135.3 (5)
O(3)–Mn(1)–N(1)	120.8 (3)	O(4)–Mn(1)–N(1)	90.4 (3)	Mn(1)–O(2)–C(2)	111.6 (5)	Mn(1)–O(3)–Mn(2)	100.2 (2)
O(1)–Mn(2)–O(3)	74.5 (2)	O(1)–Mn(2)–O(5)	87.4 (2)	Mn(1)–O(3)–C(15)	109.8 (5)	Mn(2)–O(3)–C(15)	149.7 (5)
O(1)–Mn(2)–O(7)	91.7 (2)	O(1)–Mn(2)–N(2)	177.4 (2)	Mn(1)–O(4)–C(16)	112.7 (5)	Mn(2)–O(5)–Mn(3)	101.7 (2)
O(1)–Mn(2)–N(3)	88.7 (2)	O(3)–Mn(2)–O(5)	88.8 (2)	Mn(2)–O(5)–C(29)	146.1 (4)	Mn(3)–O(5)–C(29)	111.0 (4)
O(3)–Mn(2)–O(7)	157.0 (2)	O(3)–Mn(2)–N(2)	103.5 (2)	Mn(3)–O(6)–C(30)	111.2 (5)	Mn(2)–O(7)–Mn(3)	101.1 (2)
O(3)–Mn(2)–N(3)	93.3 (2)	O(5)–Mn(2)–O(7)	72.0 (2)	Mn(3)–O(7)–C(43)	110.1 (4)	Mn(2)–O(7)–C(43)	146.6 (5)
O(5)–Mn(2)–N(2)	90.9 (2)	O(5)–Mn(2)–N(3)	174.9 (2)	O(1)–C(1)–C(2)	115.0 (6)	Mn(3)–O(8)–C(44)	111.7 (4)
O(7)–Mn(2)–N(2)	89.7 (2)	O(7)–Mn(2)–N(3)	104.8 (2)	O(3)–C(15)–C(16)	114.8 (7)	O(2)–C(2)–C(1)	116.0 (7)
N(2)–Mn(2)–N(3)	93.1 (3)	O(5)–Mn(3)–O(6)	86.1 (2)	O(4)–C(16)–C(15)	116.3 (7)	O(5)–C(29)–C(30)	115.1 (6)
O(5)–Mn(3)–O(7)	84.7 (2)	O(5)–Mn(3)–O(8)	164.5 (2)	O(6)–C(30)–C(29)	114.8 (7)	O(7)–C(43)–C(44)	115.2 (7)
O(5)–Mn(3)–N(4)	96.4 (2)	O(6)–Mn(3)–O(7)	164.8 (2)	O(8)–C(44)–C(43)	116.1 (6)		

Compound **4**

Fe(1)···Fe(1′)	3.223 (3)	Fe(2)···Fe(2′)	3.195 (3)	Fe(2)–O(3′)	2.004 (5)	Fe(2)–N(4)	2.148 (6)
Fe(1)–O(1)	2.236 (5)	Fe(1)–O(2)	1.994 (6)	Fe(2)–N(5)	2.178 (6)	O(1)–C(1)	1.338 (11)
Fe(1)–O(1′)	2.012 (6)	Fe(1)–N(1)	2.257 (6)	O(2)–C(2)	1.346 (9)	O(3)–C(30)	1.364 (12)
Fe(1)–N(2)	2.256 (6)	Fe(1)–N(3)	2.237 (7)	O(4)–C(31)	1.341 (11)	C(1)–C(2)	1.423 (9)
Fe(2)–O(3)	2.082 (6)	Fe(2)–O(4)	1.974 (6)	C(30)–C(31)	1.406 (10)		
O(1)–Fe(1)–O(2)	77.7 (2)	O(1)–Fe(1)–O(1′)	81.5 (3)	O(4)–Fe(2)–N(4)	96.7 (2)	O(4)–Fe(2)–N(5)	98.7 (2)
O(1)–Fe(1)–N(1)	167.8 (3)	O(1)–Fe(1)–N(2)	94.2 (2)	N(4)–Fe(2)–O(3′)	99.1 (2)	N(4)–Fe(2)–N(5)	94.4 (2)
O(1)–Fe(1)–N(3)	91.1 (2)	O(2)–Fe(1)–O(1′)	159.1 (2)	N(5)–Fe(2)–O(3′)	96.4 (2)	Fe(1)–O(1)–Fe(1′)	98.5 (3)
O(2)–Fe(1)–N(1)	90.1 (2)	O(2)–Fe(1)–N(2)	88.8 (2)	Fe(1)–O(1)–C(1)	109.2 (4)	Fe(1′)–O(1)–C(1)	152.2 (4)
O(2)–Fe(1)–N(3)	91.3 (2)	N(1)–Fe(1)–O(1′)	110.7 (3)	Fe(1)–O(2)–C(2)	118.1 (4)	Fe(2)–O(3)–Fe(2′)	102.8 (3)
N(1)–Fe(1)–N(2)	85.0 (2)	N(1)–Fe(1)–N(3)	89.5 (2)	Fe(2)–O(3)–C(30)	111.3 (4)	Fe(2′)–O(3)–C(30)	145.6 (5)
N(2)–Fe(1)–O(1′)	91.3 (2)	N(2)–Fe(1)–N(3)	174.5 (2)	Fe(2)–O(4)–C(31)	115.6 (4)	O(1)–C(1)–C(2)	118.4 (7)
N(3)–Fe(1)–O(1′)	90.6 (2)	O(3)–Fe(2)–O(4)	80.1 (2)	O(2)–C(2)–C(1)	116.5 (8)	O(3)–C(30)–C(31)	116.3 (8)
O(3)–Fe(2)–O(3′)	77.2 (3)	O(3)–Fe(2)–N(4)	130.4 (2)	O(4)–C(31)–C(30)	116.6 (8)		
O(3)–Fe(2)–N(5)	135.2 (2)	O(4)–Fe(2)–O(3′)	157.2 (2)				

Compound **5**

Fe(1)···Fe(2)	3.257 (2)	Fe(1)···Fe(3)	3.321 (2)	Fe(1)–O(5)	2.237 (5)	Fe(1)–O(6)	1.936 (4)
Fe(1)···Fe(4)	3.137 (2)	Fe(2)···Fe(3)	3.079 (2)	Fe(1)–N(1)	2.149 (6)	Fe(3)–O(1)	2.079 (5)
Fe(2)···Fe(4)	3.285 (2)	Fe(3)···Fe(4)	3.481 (2)	Fe(3)–O(5)	2.184 (4)	Fe(3)–O(8)	1.947 (5)
Fe(1)–O(1)	2.080 (4)	Fe(1)–O(3)	2.020 (4)	Fe(3)–O(7)	2.326 (4)	Fe(3)–N(4)	2.275 (5)

Table III (Continued)

Fe(3)–N(3)	2.156 (5)	O(1)–C(1)	1.370 (6)	O(7)–C(43)	1.377 (9)	C(15)–C(16)	1.409 (8)
O(2)–C(2)	1.344 (8)	O(4)–C(16)	1.348 (8)	C(1)–C(2)	1.416 (8)	C(43)–C(44)	1.430 (8)
O(3)–C(15)	1.381 (7)	O(6)–C(30)	1.334 (7)	C(29)–C(30)	1.399 (11)		
O(5)–C(29)	1.385 (6)	O(8)–C(44)	1.341 (8)				
O(1)–Fe(1)–O(3)	84.9 (2)	O(1)–Fe(1)–O(5)	77.6 (2)	Fe(2)–O(2)–C(2)	122.0 (3)	Fe(3)–O(1)–C(1)	128.9 (4)
O(1)–Fe(1)–O(6)	125.4 (2)	O(1)–Fe(1)–N(1)	99.6 (2)	Fe(1)–O(3)–Fe(4)	91.8 (1)	Fe(1)–O(3)–Fe(2)	104.5 (2)
O(3)–Fe(1)–O(5)	85.6 (2)	O(3)–Fe(1)–O(6)	140.8 (2)	Fe(1)–O(3)–C(15)	137.2 (4)	Fe(2)–O(3)–Fe(4)	95.4 (2)
O(3)–Fe(1)–N(1)	107.7 (2)	O(5)–Fe(1)–O(6)	78.7 (2)	Fe(4)–O(3)–C(15)	107.8 (3)	Fe(2)–O(3)–C(15)	110.9 (3)
O(5)–Fe(1)–N(1)	166.2 (2)	O(6)–Fe(1)–N(1)	92.4 (2)	Fe(1)–O(5)–Fe(3)	97.4 (1)	Fe(4)–O(4)–C(16)	121.1 (4)
O(1)–Fe(3)–O(5)	78.8 (2)	O(1)–Fe(3)–O(7)	87.7 (2)	Fe(3)–O(5)–Fe(4)	109.7 (2)	Fe(1)–O(5)–Fe(4)	93.4 (2)
O(1)–Fe(3)–O(8)	164.4 (2)	O(1)–Fe(3)–N(3)	100.7 (2)	Fe(3)–O(5)–C(29)	119.5 (3)	Fe(1)–O(5)–C(29)	107.3 (4)
O(1)–Fe(3)–N(4)	87.1 (2)	O(5)–Fe(3)–O(7)	74.7 (2)	Fe(1)–O(6)–C(30)	118.6 (5)	Fe(4)–O(5)–C(29)	122.4 (3)
O(5)–Fe(3)–O(8)	102.0 (2)	O(5)–Fe(3)–N(3)	94.7 (2)	Fe(2)–O(7)–Fe(4)	99.9 (2)	Fe(2)–O(7)–Fe(3)	90.7 (2)
O(5)–Fe(3)–N(4)	164.7 (2)	O(7)–Fe(3)–O(8)	77.6 (2)	Fe(2)–O(7)–C(43)	139.8 (3)	Fe(3)–O(7)–Fe(4)	97.8 (2)
O(7)–Fe(3)–N(3)	165.1 (1)	O(7)–Fe(3)–N(4)	99.0 (2)	Fe(4)–O(7)–C(43)	113.4 (3)	Fe(3)–O(7)–C(43)	105.7 (3)
O(8)–Fe(3)–N(3)	94.8 (2)	O(8)–Fe(3)–N(4)	90.0 (2)	O(1)–C(1)–C(2)	117.2 (6)	Fe(3)–O(8)–C(44)	118.6 (4)
N(3)–Fe(3)–N(4)	93.7 (2)	Fe(1)–O(1)–Fe(2)	94.2 (1)	O(3)–C(15)–C(16)	116.7 (5)	O(2)–C(2)–C(1)	117.9 (5)
Fe(1)–O(1)–Fe(3)	106.0 (1)	Fe(2)–O(1)–Fe(3)	87.6 (2)	O(5)–C(29)–C(30)	116.8 (5)	O(4)–C(16)–C(15)	117.3 (5)
Fe(2)–O(1)–C(1)	106.4 (3)	Fe(1)–O(1)–C(1)	121.1 (4)	O(7)–C(43)–C(44)	117.0 (6)	O(6)–C(30)–C(29)	118.3 (5)
				O(8)–C(44)–C(43)	118.4 (6)		

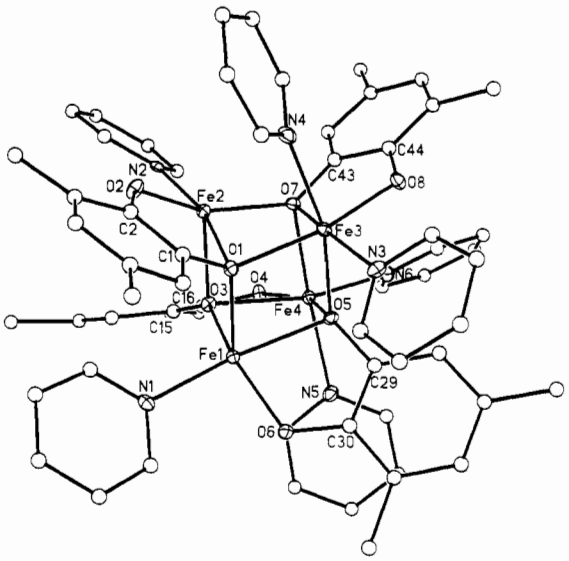

Figure 5. Computer-generated plot of the structure of **5**. Iron, oxygen, and nitrogen are shown as 30% probability thermal ellipsoids, and carbon atoms are shown as spheres of arbitrary radius. H atoms and *tert*-butyl methyls have been omitted for clarity.

distances which form part of chelate rings are consistently longer than those between monomeric units (2.315 (4) vs 2.102 (4) Å). The terminal Fe–O distances are 1.942 (4) Å. The Fe–N distances for the five-coordinate metals are significantly shorter than those for the six-coordinate irons (2.153 (6) vs 2.215 (5) Å). The tetrahedral geometry at the bridging oxygens is distorted inward toward the center of the cube, resulting in low Fe–O–Fe angles (97.4 (2)°) and large Fe–O–C angles (118.4 (3)°). O–C distances are longer for bridging oxygens (1.378 (7) Å) than for terminal oxygens (1.342 (8) Å).

Discussion

Compounds **1–5** were synthesized by a simple route as depicted by the general equation

$$M[N(SiMe_3)_2]_2 + DBCatH_2 \rightarrow (1/n)[M(DBCat)]_n + 2HN(SiMe_3)_2 \quad (1)$$

where M = Mn or Fe. This type of reaction[36] is a generally superior method for synthesizing a variety of neutral alkoxide,[31] thiolate,[37] phosphide,[38] and arsenide[38] compounds of manganese(II) and iron(II). Previous syntheses of catecholate and semiquinonate complexes of transition metals generally have employed either ligand-exchange reactions between alkali metal salts (or basic solutions) of catechol and a variety of transition metal salts (e.g., $Fe(SO_4)$,[39] $MnCl_2$,[21] $Mn(acac)_3$[28]) or oxidation of metal carbonyls with quinones. Initial results with $Co[N(SiMe_3)_2]_2$ and $DBCatH_2$, which afforded the complex $[Co_4(3,5\text{-}t\text{-}Bu_2C_6H_2O_2)_4(THF)_{5.5}]$,[32] suggested that a range of new compounds might be accessible starting from the manganese and iron amides. At first, reactions analogous to the synthesis of $[Co_4(3,5\text{-}t\text{-}Bu_2C_6H_2O_2)_4(THF)_{5.5}]$ for Mn and Fe were attempted in THF. The use of THF as solvent with 3,5-di-*tert*-butylcatechol and iron amide gave a product which was isostructural with the cobalt tetramer but which was badly disordered and could not be refined to a satisfactory level. In the case of the analogous reaction with manganese amide, no crystalline product could be obtained in THF. In the absence of donor solvents, no crystalline products could be obtained for either manganese or iron. Pyridine was chosen as an alternative solvent due to its strong donor ability and its rigidity, which would help eliminate the disorder problems encountered with THF adducts.

The use of pyridine as solvent in reaction 1 affords the dimeric catecholate derivatives of manganese(II) and iron(II) **1** and **4**. Dimeric catecholate compounds have been structurally characterized for molybdenum,[40–42] tungsten,[43] and copper[23] but not for manganese or iron. A similar dimeric compound, bis[(μ-1,1′-biphenyl-2,2′-diolato-O,μ-O')(1,1′-biphenyl-2,2′-diolato-O,O')-iron(III)],[44] has been structurally characterized. Dimeric structures have been postulated for the M^{II} semiquinonates $[Mn_2(2\text{-acetyl-}1,4\text{-benzosemiquinonate})_4L_2]$ (L = DME, CH_3CN, CO)[45] and $[Fe(DBSQ)_2(\text{bidentate nitrogen base})]$[46] on the basis of EPR and magnetic susceptibility measurements. The manganese(II) tetramer $Mn_4(DBSQ)_8$ and its pyridine adduct, the Mn(IV) monomer $Mn(DBCat)_2(py)_2$, have been structurally

(36) Lappert, M. F.; Power, P. P.; Sanger, A. R.; Srivastava, R. C. *Metal and Metalloid Amides*; Ellis Horwood: Chichester, U.K., 1980; Chapter 11.
(37) Power, P. P.; Shoner, S. C. *Angew. Chem., Int. Ed. Engl.* **1991**, *30*, 330.
(38) Chen, H.; Olmstead, M. M.; Pestana, D. C.; Power, P. P. *Inorg. Chem.* **1991**, *30*, 1783.
(39) Garge, P.; Chikate, R.; Padhye, S.; Tuchagues, J.-P. *Inorg. Chim. Acta* **1989**, *157*, 239.
(40) Pierpont, C. G.; Downs, H. H.; Rukavina, T. G. *J. Am. Chem. Soc.* **1974**, *96*, 5573.
(41) Atovmyan, L. O.; Tkachev, V. V.; Shishova, T. G. *Dokl. Akad. Nauk SSSR* **1972**, *205*, 609.
(42) Buchanan, R. M.; Pierpont, C. G. *Inorg. Chem.* **1979**, *18*, 1616.
(43) deLearie, L. A.; Pierpont, C. G. *Inorg. Chem.* **1988**, *27*, 3842.
(44) Ainscough, E. W.; Brodie, A. M.; McLachlan, S. J.; Brown, K. L. *J. Chem. Soc., Dalton Trans.* **1983**, 1385.
(45) Mathur, P.; Dismukes, G. C. *J. Am. Chem. Soc.* **1983**, *105*, 7093.
(46) Lynch, M. W.; Valentine, M.; Hendrickson, D. N. *J. Am. Chem. Soc.* **1982**, *104*, 6982.

Table IV. Selected Bond Lengths (Å) for Various Mn, Fe, and Co Catecholate and Semiquinonate Complexes

	$Mn_2(DBCat)_2(py)_6^a$ (1)	$Mn_4(DBCat)_4(py)_6^a$ (2)	$Mn_3(DBCat)_4(py)_4^a$ (3)	$[Mn_2(Br_4Cat)_4(OPPh_3)]^{2-b}$	$Mn(DBCat)_3^{2-c}$	$Mn_4(DBSQ)_8^d$	$Mn(DBCat)_2(py)_2^d$	$Mn(phth)_2(py)_2^e$
M–O(av)	2.087 (2) (t)	2.032 (4) (t)	1.869 (6) (t)	1.899 (13) (t)	1.907 (3)	2.095 (6) (t)	1.854 (2)	2.230 (4) (Quin)
	2.139 (2) (μ_2-br)	2.154 (4) (μ_2-br)	1.911 (5) (μ_2-br)	1.909, 2.723 (μ_2-br)		2.165 (8) (μ_2-br)		2.100 (3) (Phenox)
		2.215 (4) (μ_3-br)	2.194 (5) (μ_2-br)			2.309 (7) (μ_3-br)		
C–O(av)	1.339 (4) (t)	1.349 (7) (t)	1.362 (10) (t)	1.340 (22) (t)	*k*	1.288 (14) (t)	1.349 (4)	1.217 (6) (Quin)
	1.353 (3) (μ_2-br)	1.358 (7) (μ_2-br)	1.379 (9) (μ_2-br)	1.348 (22) (μ_2-br)		1.297 (11) (μ_2-br)		1.298 (5) (Phenox)
		1.376 (7) (μ_3-br)				1.290 (9) (μ_3-br)		
OC–CO(av)	1.421 (5)	1.417 (8)	1.405 (10)	1.415 (25)	*k*	1.455 (17)	1.402 (4)	1.495 (7)

	$Fe_2(DBCat)_2(py)_6$/ $Fe_2DBCat)_2(py)_4^a$ (4)	$Fe_4(DBCat)_4(py)_6^a$ (5)	$Fe(phth)_2(H_2O)_2^f$	$Fe_4(DBSQ)_4(DBCat)_4^g$ (Cat)	$Fe_4(DBSQ)_4(DBCat)_4^g$ (SQ)	$Fe(Cat)_3^{3-h}$	$Fe(DBSQ)_3^g$	$Fe(PhenSQ)_3$· PhenQ[i]	$Co_4(DBCat)_4(THF)_{5.5}^j$
M–O(av)	1.984 (6) (t)	1.942 (4) (t)	2.143 (4) (Quin)	1.868 (4) (t)	2.016 (4) (t)	2.015 (6)	2.015 (2)	2.027 (3)	1.916 (14) (t)
	2.084 (6) (μ_2-br)	2.173 (4) (μ_3-br)	2.045 (4) (Phenox)	2.000 (4) (μ_2-br)	2.119 (4) (μ_2-br)				2.107 (11) (μ_3-br)
				2.183 (4) (μ_3-br)					
C–O(av)	1.344 (10) (t)	1.342 (8) (t)	1.236 (6) (Quin)	1.345 (6) (t)	1.283 (8) (t)	1.338 (9)	1.281 (3)	1.283 (5)	1.34 (2) (t)
	1.351 (12) (μ_2-br)	1.378 (7) (μ_3-br)	1.298 (6) (Phenox)	1.378 (6) (μ_2-br)	1.310 (6) (μ_2-br)				1.39 (2) (μ_3-br)
				1.387 (5) (μ_3-br)					
OC–CO(av)	1.415 (10)	1.414 (9)	1.502 (7)	1.387 (8)	1.456 (10)	1.409 (12)	1.452 (4)	1.435 (7)	1.412 (22)

[a] This work. [b] Reference 19. [c] Reference 28. [d] Reference 21. [e] Reference 47. [f] Reference 48. [g] Reference 26. [h] Reference 29. [i] Reference 30. [j] Reference 32. [k] Not available.

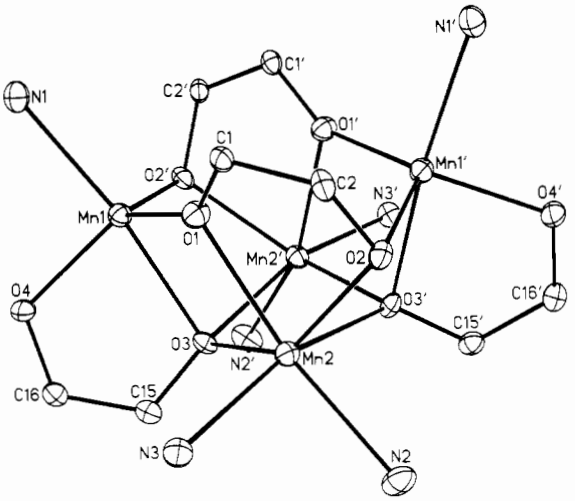

Figure 6. View of the core atoms of **2**.

characterized.[21] Structures similar to this Mn(IV) compound have been obtained using Lawsone (*o*-hydroxy-*p*-naphthoquinone) giving the Mn(II) and Fe(II) phenoxy/quinone compounds $Mn(phth)_2(py)_2$[47] and $Fe(phth)_2(H_2O)_2$.[48] Important structural parameters for these and other relevant quinone, semiquinonate, and catecholate compounds are summarized in Table IV. C–O distances are considered diagnostic of the oxidation state of 1,2-benzodioxy ligands. Catecholate C–O distances are generally in the range 1.34–1.39 Å, those of semiquinonates are shorter at 1.28–1.31 Å, and quinone C–O distances are shortest at ca. 1.23 Å. C(1)–C(2) ring distances follow the reverse pattern, with catecholates having much shorter C–C distances (ca. 1.40 Å) than quinones (ca. 1.50 Å).[27] From these considerations, it is clear that the C–O and C–C distances in **1** and **4** fall into the catecholate range.

The bridging geometry in semiquinonate and catecholate dimers of manganese and iron has been the subject of some speculation. Two possibilities have been proposed. In one case, the metal centers are each bonded to different oxygens of a single catecholate ligand, giving a M–O–C–C–O–M bridging unit. Previously structurally characterized dimers of this type include the compounds $M_2(o\text{-}Cl_4Cat)_6$ (M = Mo,[40] W[43]) and the copper(II) complex $Cu_2(Xyl\text{-}o)(o\text{-}Cl_4Cat)$.[49] In the second case, the bridging catecholate has one doubly bridging oxygen and one terminal O. This type of bridging is found in **1** and **4**, which suggests that this bridging mode may also be preferred by other manganese and iron catecholate or semiquinonate or semiquinonate dimers in the solid state.

With lower pyridine concentrations, compounds **2** and **5** are formed. Although **2** may be formed by simple recrystallization of **1** in toluene, this method does not work with the corresponding iron complex. Nevertheless, both compounds may be synthesized in high yield by stoichiometric reactions of $[M(DBCat)]_x$ with pyridine in hydrocarbon solvent. Variations in the stoichiometry of M:py (1:1 up to 4:1) give **2** and **5** in varying yields.

The core atoms of compounds **2** and **5** are displayed in Figures 6 and 7. Complex **5** has a M_4O_4 core very similar to that previously observed for $[Co_4(DBCat)_4(THF)_{5.5}]$[32] and has some structural similarity to the extensively studied Fe_4S_4 cluster observed in various proteins.[50] The core of **2**, however, is quite different. This complex contains two catechol ligands each bridging three metals via two doubly bridging oxygens. This is

(47) Mulay, M. P.; Garge, P. L.; Padhye, S. B.; Haltiwanger, R. C.; de-Learie, L. A.; Pierpont, C. G. *J. Chem. Soc., Chem. Commun.* **1987**, 581.
(48) Garge, P.; Chikate, R.; Padhye, S.; Savariault, J.-M.; de Loth, P.; Tuchagues, J.-P. *Inorg. Chem.* **1990**, *29*, 3315.
(49) Karlin, K. D.; Gultneh, Y.; Nicholson, T.; Zubieta, J. *Inorg. Chem.* **1985**, *24*, 3725.
(50) Holm, R. H. *Chem. Soc. Rev.* **1981**, *10*, 455. See also: Que, L., Jr., Ed. *Metal Clusters in Proteins*; ACS Symposium Series 372; American Chemical Society: Washington, DC, 1988.

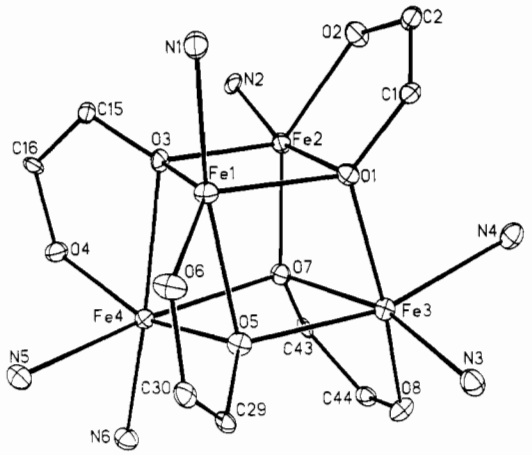

Figure 7. View of the core atoms of **5**.

the first example of this type of bridging by catechols to be structurally characterized. The potential to form this type of bridge bond was recognized for the dimer $Mo_2(o\text{-}Cl_4Cat)_6$, although attempts to synthesize $M_3(\mu^2,\mu^2\text{-Cat})_2$ from $Mo_2(o\text{-}Cl_4Cat)_6$ were, apparently, unsuccessful.[40] The cluster bonding in **2** is completed by two catecholates with the same terminal μ_3-bridging geometry taken up by the catecholate ligands in **5** and $[Co_4(DBCat)_4(THF)_{5.5}]$,[32] which gives **2** a basket-like appearance. This overall geometry is unique for a tetramanganese cluster and, to our knowledge, has not been observed for any tetrametallic cluster. Currently known tetramanganese clusters generally have adamantane,[51] cubane,[52-55] or butterfly type[56] configurations. The known tetrametallic semiquinonate complexes, including $M_4(DBSQ)_8$ (M = Mn,[21] Co,[22] Ni[22]) and $Fe_4(DBSQ)_4(DBCat)_4$,[26] have planar metal arrangements with triply bridging terminal and doubly bridging terminal semiquinonates or catecholates. It is unclear why **2** prefers this unusual M_4O_6 geometric isomer over the more typical M_4O_4 cubane geometry of **5**.

Slow oxidation of **2** over the course of several weeks affords **3**, the first example of a catecholate complex with mixed valence at the metals. Examination of the stoichiometry of this oxidation reveals the loss of a $Mn(py)_2$ unit from the tetramer **2**. One possible reaction that could account for this is

$$Mn_4(DBCat)_4(py)_6 + O_2 \rightarrow Mn_3(DBCat)_4(py)_4 + [MnO_2(py)_2]_x \quad (2)$$

The side product $[MnO_2(py)_2]_x$ of this reaction may explain a substantial portion of the uncharacterized insoluble dark powder also obtained in this reaction. The product **3** may also be obtained in higher yield via the route

$$3[Mn(DBCat)] + DBQ + 4py \rightarrow Mn_3(DBCat)_4(py)_4 \quad (3)$$

The success of this reaction indicates that it may be possible to synthesize a wide range of similar compounds with various ratios of manganese to quinone giving a variety of manganese-oxidation-state combinations.

A careful examination of bond distances allows a determination of the oxidation states of the ligands and metal centers in **3** to be made. First, the C–O (1.375 (10) Å) and OC–CO (1.405 (10) Å) distances indicate that the ligands are in the catecholate (−2) and not the semiquinonate (−1) form. Thus the oxidation states for the three metals that are most likely are (2Mn(III), Mn(II)) or (Mn(IV), 2Mn(II)). Comparison of the Mn–O distances shows that they fall into two categories: bonds to the terminal metals (1.880 (6) Å) and much longer bonds to the central metal (2.194 (5) Å). From a comparison of these to other catecholate compounds in Table IV, it is clear that these distances are closest to the values for manganese(III) (1.904 (13) Å for $[Mn_2(Br_4Cat)_4(OPPh_3)]^{2-}$)[19] and manganese(II) (e.g., 2.154 (4) Å for doubly bridging distances in **2**). We can therefore assign the metal oxidation states in the complex as Mn(III)–Mn(II)–Mn(III). This arrangement of oxidation states is similar to that found in another structurally characterized compound, the trinuclear (2Mn(III), Mn(II)) species $[Mn_3(SALADHP)_2(OAc)_4)(CH_3OH)_2]$,[57] which has a linear array of metals rather than the bent configuration in **3**. A comparison may also be made between **3** and several structurally characterized Mn(II/III) binuclear complexes with phenoxy bridges similar to **3**.[58-64] The similarity of the Mn(II)–O (2.209 Å (av)) and Mn(III)–O (1.930 Å (av)) bridging distances in these compounds to those in **3** also supports the oxidation-state assignments in **3**.

Spectroscopic Studies. The EPR spectrum of **1** supports the notion that some structural aspects of catecholate dimers are shared with the semiquinone dimers. The spectrum of **1** in pyridine is almost identical to the spectrum of $[Mn_2(2\text{-acetyl-1,4-benzosemiquinonate})_4L_2]$ (L = DME, CH_3CN, CO) at 11 K in acetonitrile or DME.[45] The major difference between the two spectra is the lack of the well-defined hyperfine coupling (constant = 45 G) in **1** which in $[Mn_2(2\text{-acetyl-1,4-benzosemiquinonate})_4L_2]$ was attributed to the electron-spin-exchange interaction of two magnetically equivalent high-spin Mn(II) ions.[45] Some spectra of **1** showed this hyperfine interaction weakly, but the effect was not consistent and seemed to be concentration dependent, although no quantitative concentration study was carried out. The relative intensity of the central six-line signal, which may be attributed to the monomeric form of **1**, to that of the broader signals is also condition dependent. One explanation for this behavior is the equilibrium

$$Mn_2(DBCat)_2(py)_6 \underset{-py}{\overset{+py}{\rightleftharpoons}} 2Mn(DBCat)(py)_4 \quad (4)$$

which may be driven to the right by low Mn:py ratios. A reaction of this type may also be responsible for the single sharp EPR signal obtained for **4** in pyridine, which showed no evidence of the iron–iron interactions that might be expected in an Fe(II)–Fe(II) dimer. The EPR signals of the tetramers **2** and **5** were broad but lacked hyperfine structure, probably due to a number of different overlapping couplings.

The lack of an EPR signal for **3** was unexpected. Since the $S = 2$, $S = {}^5/_2$, $S = 2$ spin system contains an odd number of electrons, there should be no coupling which leads to a diamagnetic system even at low temperature. A comparison of this result to literature reports on EPR spectroscopic results for other similar systems showed that the closely related systems $Mn_4(DBSQ)_8$,[21]

(51) Wieghardt, K.; Bossek, U.; Gebert, W. *Angew. Chem., Int. Ed. Engl.* **1983**, *22*, 328.
(52) Bashkin, J. S.; Chang, H.-R.; Streib, W. E.; Huffman, J. C.; Hendrickson, D. N.; Christou, G. *J. Am. Chem. Soc.* **1987**, *109*, 6502.
(53) McKee, V.; Shepard, W. B. *J. Chem. Soc., Chem. Commun.* **1985**, 158.
(54) Li, Q.; Vincent, J. B.; Libby, E.; Chang, H.-R.; Huffman, J. C.; Boyd, P. D. W.; Christou, G.; Hendrickson, D. N. *Angew. Chem., Int. Ed. Engl.* **1988**, *27*, 1731.
(55) Wang, S.; Folting, K.; Streib, W. E.; Schmitt, E. A.; McCusker, J. K.; Hendrickson, D. N.; Christou, G. *Angew. Chem., Int. Ed. Engl.* **1991**, *30*, 305.
(56) Vincent, J. B.; Christmas, C.; Chang, H.-R.; Li, Q.; Boyd, P. D. W.; Huffman, J. C.; Hendrickson, D. N.; Christou, G. *J. Am. Chem. Soc.* **1989**, *111*, 2086.
(57) Li, X.; Kessissoglou, D. P.; Kirk, M. L.; Bender, C. J.; Pecoraro, V. L. *Inorg. Chem.* **1988**, *27*, 1.
(58) Wieghardt, K. *Angew. Chem., Int. Ed. Engl.* **1989**, *28*, 1153.
(59) Suzuki, M.; Mikuriya, M.; Murata, S.; Uehara, A.; Oshio, H.; Kida, S.; Saito, K. *Bull. Chem. Soc. Jpn.* **1987**, *60*, 4305.
(60) Diril, H.; Chang, H.-R.; Zhang, X.; Larsen, S. K.; Potenza, J. A.; Pierpont, C. G.; Schugar, H. J.; Hendrickson, D. N.; Isied, S. S. *J. Am. Chem. Soc.* **1987**, *109*, 6207.
(61) Buchanan, R. M.; Oberhausen, K. J.; Richardson, J. F. *Inorg. Chem.* **1988**, *27*, 971.
(62) Bashkin, J. S.; Schake, A. R.; Vincent, J. B.; Chang, H.-R.; Li, Q.; Huffman, J. C.; Christou, G.; Hendrickson, D. N. *J. Chem. Soc., Chem. Commun.* **1988**, 700.
(63) Chang, H.-R.; Diril, H.; Nilges, M. J.; Zhang, X.; Potenza, J. A.; Schugar, H. J.; Hendrickson, D. N.; Isied, S. S. *J. Am. Chem. Soc.* **1988**, *110*, 625.
(64) Chang, H.-R.; Larsen, S. K.; Boyd, P. D. W.; Pierpont, C. G.; Hendrickson, D. N. *J. Am. Chem. Soc.* **1988**, *110*, 4565.

$Mn(DBSQ)_2(py)_2$,[21] $Fe(DBSQ)(DBCat)(bpy)$,[45] and $Fe(PhenSQ)(PhenCat)(bpy)\cdot{}^1/_2PhenQ$[45] also show no EPR signal in toluene solution or glass. The reason proposed for this is the strong interaction between the electronic levels on the $S = {}^5/_2$ metals (Mn(II), Fe(III) high spin) and the nearly equivalent levels on the $S = {}^1/_2$ semiquinonate ligands.[45] Thus one plausible explanation for the lack of an EPR signal for **3** is a shift in oxidation state when the compound is in solution to give the all-Mn(II) semiquinonate form $Mn_3(DBSQ)_2(DBCat)_2(py)_4$, in which the Mn(II) ions and the semiquinonate ligands interact to quench the EPR signal. This type of oxidation-state interchange has been previously observed for the systems $Mn^{II}(DBSQ)_2(py)_2/Mn^{IV}(DBCat)_2(py)_2$[21] and $Co^{II}(DBSQ)_2(bpy)/Co^{III}(DBSQ)(DBCat)(bpy)$.[65] In both of these cases the metal centers are in the higher oxidation state in the solid and low-temperature solution and in the lower oxidation state at room temperature in solution. Other closely related compounds are $M^{II}(phth)_2(L)_2$ (M = Mn, L = py;[47] M = Fe, L = H_2O[48] (phth = phthiocolato (2-methyl-3-hydroxy-1,4-naphthoquinonato)) which have quinone and phenoxide groups in ortho positions with respect to each other. These compounds do not exhibit this electron-transfer interaction and are always in the lower of the possible metal oxidation states. Thus **3** falls closest to the general category of complexes of the form $M(Q)_2(N\ donor)_2$ (where Q = quinonoid ligand),[21] of which several examples are known where M = Cr → Ni;[65-67] however, **3** is the first example of the stoichiometry $M_3Q_4N_4$.

The UV-visible spectrum of **3** also indicates that oxidation state II prevails for manganese in solution. The dark green-brown crystals of **3** dissolve in toluene to give a light yellow solution similar in appearance to **1** and **2**. Only a single weak absorption is observed below 33 000 cm^{-1} which is characteristic of Mn(II) compounds. The recently reported compound $Mn(PhenSQ)_2(TMEDA)$ had a quite similar spectrum, with one weak absorption in the same region (25 300 vs 26 300 cm^{-1} for **3**).[68]

In summary, the structures of several new manganese and iron catecholate complexes have been described. Furthermore, the utility of the synthetic route involving the reaction of $M[N(SiMe_3)_2]_2$ with catechol for the investigation of metal quinone complex chemistry has been demonstrated. Future work will include more detailed magnetic and redox studies of these compounds as well as the characterization of other oxidation products of manganese and iron catecholates.

Acknowledgment. We thank the donors of the Petroleum Research Fund, administered by the American Chemical Society, for financial support. We also thank Professor R. D. Britt and B. E. Sturgeon for experimental assistance.

Registry No. **1**, 138982-85-1; **2**, 138982-86-2; **3**, 138956-47-5; **4**, 138956-50-0; **5**, 138982-87-3.

Supplementary Material Available: Full tables of structural parameters and refinement data atom coordinates, bond distances and angles, hydrogen coordinates, and anisotropic thermal parameters (59 pages); listings of structure factors (202 pages). Ordering information is given on any current masthead page.

(65) Buchanan, R. M.; Pierpont, C. G. *J. Am. Chem. Soc.* **1980**, *102*, 4951.
(66) Buchanan, R. M.; Clafin, J.; Pierpont, C. G. *Inorg. Chem.* **1983**, *22*, 2552.
(67) Lynch, M. W.; Buchanan, R. M.; Pierpont, C. G.; Hendrickson, D. N. *Inorg. Chem.* **1981**, *20*, 1038.
(68) Döring, M.; Waldbach, T. *Z. Anorg. Allg. Chem.* **1989**, *577*, 93.

Contribution from the Department of Chemical and Biological Sciences, Oregon Graduate Institute of Science and Technology, 19600 N.W. von Neumann Drive, Beaverton, Oregon 97006-1999

Pathways for Water Oxidation Catalyzed by the $[(bpy)_2Ru(OH_2)]_2O^{4+}$ Ion

James K. Hurst,* Jinzhong Zhou, and Yabin Lei

Received April 11, 1991

Resonance Raman (RR) spectra of the (μ-oxo)bis[*cis*-aquabis(2,2'-bipyridine)ruthenium(III)] ion and its congeners in thermodynamically accessible III-IV, IV-V, and V-V higher oxidation states have been obtained in aqueous solutions under a wide range of medium conditions. The RR spectra were dominated by single bands at 370-403 cm^{-1}, assignable to the Ru-O-Ru symmetric stretching mode (ν_s) on the basis of their ^{18}O-isotope induced shifts. From the magnitudes of the shifts, the Ru-O-Ru angles were calculated to be 155-180° for the various oxidation states. A band appearing at 812 cm^{-1} in the V-V ion which shifted to ~780 cm^{-1} in $[^{18}O]H_2O$ was assigned to a Ru=O stretching mode of a terminal oxo ligand. Below pH 0.3 the bridging μ-oxo atom became protonated; for the other ions, hydrogen bonding to the bridge was indicated by D_2O-induced solvent shifts in ν_s(Ru-O-Ru). An ^{18}O-isotope labeling study of the water oxidation reaction established the existence of a pathway in which one atom of O_2 was obtained from an aqua ligand. These results combined with published rate data suggest that this pathway involves solvent nucleophilic attack of a terminal oxo atom as the critical oxygen-oxygen bond forming step, with the bridging oxygen atom serving the essential role of activating and/or orienting the reactant H_2O through formation of a strong hydrogen bond. A second major pathway, for which both O atoms were derived from solvent, was also identified, but no definitive evidence was obtained for a pathway for which both O atoms originated in coordinated H_2O.

Introduction

Dimeric ruthenium complexes of the type $(L_2Ru(OH_2))_2O$, where L is 2,2'-bipyridine[1-3] or a ring-substituted analogue,[4,5] display unique catalytic capabilities for water oxidation, both electrochemically and in reactions with strong oxidants in homogeneous solution. These reactions have considerable intrinsic interest, e.g., in understanding how redox metal clusters can overcome kinetic barriers imposed by reactant noncomplementarity and as potential models for biological water oxidation;[5-7] they might also find essential technological roles, e.g., as catalysts for oxidative half-cycles in practical water photolysis systems.[8,9] Nonetheless, their reactivity is presently poorly described, with

* To whom correspondence should be addressed.

(1) Gilbert, J. A.; Eggleston, D. S.; Murphy, W. R., Jr.; Geselowitz, D. A.; Gersten, S. W.; Hodgson, D. W.; Meyer, T. J. *J. Am. Chem. Soc.* **1985**, *107*, 3855.
(2) Honda, K.; Frank, A. J. *J. Chem. Soc., Chem. Commun.* **1984**, 1635.
(3) Collin, J. P.; Sauvage, J. P. *Inorg. Chem.* **1986**, *25*, 135.
(4) Rotzinger, F. P.; Munavalli, S.; Comte, P.; Hurst, J. K.; Gratzel, M.; Pern, F.-J.; Frank, A. J. *J. Am. Chem. Soc.* **1987**, *109*, 6619.
(5) Comte, P.; Nazeeruddin, M. K.; Rotzinger, F. P.; Frank, A. J.; Gratzel, M. *J. Mol. Catal.* **1989**, *52*, 63.
(6) See, e.g.: Weighardt, K. *Angew. Chem., Int. Ed. Engl.* **1989**, *28*, 1153 and references cited therein.
(7) Geselowitz, D.; Meyer, T. J. *Inorg. Chem.* **1990**, *29*, 3894.

0020-1669/92/1331-1010$03.00/0